Tellus (1993), 45A, 539–557
Printed in Belgium - all rights reserved

TELLUS
ISSN 0280-6495

Comparison of initial and lateral boundary condition sensitivity for a limited-area model

By RONALD M. ERRICO*, TOMISLAVA VUKIĆEVIĆ, and KEVIN RAEDER, *National Center for Atmospheric Research*[1], *Boulder, Colorado 80307–3000, USA*

(Manuscript received 9 November 1992; in final form 23 april 1993)

ABSTRACT

The sensitivities of two forecast aspects with respect to perturbations of initial and lateral boundary conditions are determined using an adjoint of a limited-area model. Sensitivities are presented as gradient fields. Some characteristics of the sensitivity fields have simple dynamical explanations, such as their strong dependence on winds, and do not require an adjoint model to reveal them. Other characteristics would be difficult to ascertain without an adjoint model, although they, too, in retrospect, have simple dynamical explanations. Still others, although equally important and undoubtedly dependent on the dynamics, would be practically impossible to determine without an adjoint. The quantity and quality of information provided by the adjoint solutions render the adjoint model a tool that is indispensable for sensitivity analysis.

1. Introduction

Limited-area forecast or simulation models are used in many areas of meteorological research. All such models require specification of lateral boundary conditions (LBCs) using some source external to the model, unless horizontal periodicity of the fields is imposed. In many mesoscale models of real events, the LBCs are specified from either a temporal sequence of analyses near the boundary or from forecast fields obtained from a model whose domain is larger.

There is much evidence that, for some widely used combinations of domain size and forecast period, forecasts are more sensitive to LBC specification than to initial condition (IC) specification within the model domain (Vukićević and Errico, 1990). This is to be expected because as time advances, features are advected from inflow boundaries into the interior as interior features exit at the outflow boundaries. This behavior has important implications for proper design and interpretation of predictability studies (Errico and Baumhefner, 1987) and observation system simulation experiments (OSSEs) using limited-area models.

Typically, the dependence of forecasts on either LBCs or ICs is measured by performing an impact study: a "control" forecast is made, then a specific perturbation to the LBC or IC is introduced, a second forecast is made with the perturbed conditions, and finally the two results are compared. A significant limitation of this type of sensitivity analysis and its subsequent interpretation is that it really only yields the effects of one single perturbation (or a single ensemble of perturbations if several perturbations are considered). It is likely that significantly different results can be produced by different perturbations (e.g., by using a different sequence of random numbers drawn from the same distribution if the perturbations are generated using random numbers). An example in the context of predictability experiments is presented by Vukićević and Errico (1990), and further evidence of the severity of this limitation will be presented here.

[1] The National Center for Atmospheric Research is sponsored by the National Science Foundation.

* Corresponding author.

Another, more general method of sensitivity analysis uses an adjoint model to determine the gradient of a forecast aspect with respect to LBCs or ICs (Errico and Vukićević, 1992; Hall and Cacuci, 1983). For this analysis, actual fields of sensitivity are produced, and therefore, the results apply to any arbitrary perturbation (if not too large). Limitations of the method include approximations introduced through linearization (Errico et al., 1993; Vukićević and Errico, 1993) and restriction of each result to one family of forecast aspects; i.e., the sensitivity obtained applies to all perturbations with respect to one aspect unlike the impact study that is informative for all aspects given one perturbation (Hall et al., 1982). This latter limitation may not be severe if only qualitative statements regarding sensitivity are to be extracted from the results since, in many cases, several aspects may be determined by a single physical process (e.g., both rms forecast errors and cyclone depth may be determined by baroclinic instability) yielding similar characteristics of sensitivity.

In the analysis performed here, the adjoint technique for sensitivity determination is used following Errico and Vukićević (1992). Questions to be answered include: (1) How do the sensitivities with respect to possible IC and LBC perturbations compare as a function of forecast time? (2) How do the sensitivities on the boundary compare for various fields, distance from edge, and location (e.g., upstream and downstream boundaries)? (3) How do the boundary sensitivities depend on synoptic situation along the boundary (in particular, the strength of advection)? and (4) How do the boundary sensitivities depend on the aspect measured? Some of these questions should have answers expected from simple consideration of (advection) characteristics. Others may not be as straightforward, and even those that primarily depend on advection may not be obvious since, for the realistic fields we will consider, the advection and wave propagation characteristics do not have simple configurations.

The purpose of this report is to describe some of the general properties of adjoint fields as an aid to future interpretation and as a stimulus for new research applications. Consistent with this purpose, we consider a single, commonly used LBC formulation (the Davies and Turner, 1977 scheme) and examine two forecast aspects. The examples are chosen for their demonstrative value rather than as an attempt at solving some current problem. Only what appear to be the most general results are described along with some specific results of interest.

The model, its LBC formulation, and their adjoints are described in Section 2. The synoptic cases and forecast aspects considered are described in Section 3. Results are presented in Sections 4 and 5 and summarized in Section 6.

2. Model

The model used in this study is a dry version of the Pennsylvania State University/National Center for Atmospheric Research (PSU/NCAR) mesoscale model (denoted MM4). It is a limited-area, primitive equation model in flux form. It is described fully in Anthes et al. (1987). The vertical coordinate is $\sigma = (p - p_t)/p^*$, with $p^* = p_s - p_t$ for p pressure and subscripts s and t denoting surface and top values, respectively ($p_t = 100$ hPa in the experiments here). Horizontal and vertical diffusion are included, along with a bulk aerodynamic formulation of the planetary boundary layer and a prognostic equation for ground temperature. A dry version is used because the accurate treatment of an adjoint for highly nonlinear and discontinuous moist parameterization schemes remains to be developed.

The MM4 LBC scheme is the sponge region, relaxation scheme of Davies and Turner (1977). For each of the model prognostic variables p^*u, p^*v, p^*T, p^* (where u, v, and T are eastward and northward wind components and temperature, respectively), relaxation terms of the form

$$f(t+2\,\Delta t) - f(t) = \cdots + 2w_n\beta\,\Delta t \times [f_e(t) - f(t) - \gamma\,\nabla^2(f_e(t) - f(t))] \tag{1}$$

are added to the prognostic equations, where f denotes a generic model prognostic variable, t denotes time, Δt denotes a model time step, subscript e denotes an externally prescribed value, β is a scaling parameter, γ is a smoothing coefficient, ∇^2 is a finite difference form of the Laplace operator applied on the model σ-surfaces, and w_n is a weighting function that depends only on the number (n) of grid points from the nearest boundary edge

$$w_n = \begin{cases} \dfrac{5-n}{3}, & \text{if } n = 2, 3, 4, \\ 0, & \text{if } n > 4. \end{cases} \tag{2}$$

For $n = 1$ (the grid edge), $f = f_e$. The values of f_e we use are linearly interpolated in time between 12-hourly fields ($\tilde{f}$) provided by either an analysis or forecast from a larger domain model:

$$f_e = \frac{(t_2 - t)\,\tilde{f}(t_1) + (t - t_1)\,\tilde{f}(t_2)}{t_2 - t_1}, \tag{3}$$

where $t_1 \leqslant t < t_2$ for time t and specification times t_1 and $t_2 = t_1 + 12$ h.

The adjoint for the MM4 has been developed following the procedure in Errico and Vukićević (1992), except with fewer approximations or changes to the MM4 equations. In particular, the new adjoint considers the equations in their original flux form and is the exact adjoint of the dry MM4 with the following four exceptions:

(1) Perturbations of the coefficients of the Richardson-number dependent vertical diffusion are ignored. Actually, these coefficients often have their maximum or minimum permitted values, implying that their perturbations are in fact zero, so this approximation is often negligible in practice.

(2) Perturbations of p^* are ignored in the determination of the difference between potential temperatures of the ground and the lowest model level that is used to calculate the diabatic vertical fluxes of u, v, and T. Perturbations of the surface pressure used to convert temperature to potential temperature are considered for other terms.

(3) There is no consideration of dry convective adjustment, although it can occur in the MM4. In many cases it occurs infrequently or not at all.

(4) The basic state used to compute the coefficients is varied discontinuously by periodically reading fields from a stored file. The coefficients are held constant between these periodic basic state update times. Since the MM4 time step is determined by numerical stability considerations and the short spatial scales often considered require very short time steps, the storage and input of all fields at every time step for an extended period is a prohibitive cost on most existing computer systems. Additionally, some computational savings are obtained since all coefficients need not be recomputed every time step.

The adjoint model takes as input the gradient of some function J with respect to the forecast model state at the verification time, where J is a quantitative measure of some forecast aspect to be examined (some examples appear in Section 3). The adjoint model then outputs fields of the gradient of J with respect to both IC and LBC fields at earlier times. The interpretation of these fields is that

$$\Delta J \approx \sum_i \frac{\partial J}{\partial f_i} f_i', \tag{4}$$

where ΔJ is the change of J between two model forecasts, the second of which has ICs or LBCs perturbed by f_i', where f_i denotes any model variable IC or LBC (defined discretely in space), and the summation runs over all such variables. The approximation eq. (4) is the first-order variation of J with respect to the controlling variables f_i and is asymptotically exact as $|f_i'| \to 0$ for all i.

The computation of $\partial J/\partial f_i$ for IC fields is described in Errico and Vukićević (1992). Computation for LBC fields follows the adjoints of eq. (1) and eq. (3), yielding, e.g.,

$$\frac{\partial J}{\tilde{f}(t_2)} = 2 w_n \beta\, \Delta t \left[\sum_{t_m = t_1}^{t_2} \frac{t_m - t_1}{t_2 - t_1} \left(\frac{\partial J}{\partial f} - \gamma\, \nabla^{2\mathrm{T}} \frac{\partial J}{\partial f} \right) + \sum_{t_m = t_2}^{t_3} \frac{t_3 - t_m}{t_3 - t_2} \left(\frac{\partial J}{\partial f} - \gamma\, \nabla^{2\mathrm{T}} \frac{\partial J}{\partial f} \right) \right], \tag{5}$$

where t_m is a discrete model time, $t_3 = t_2 + 12$ h, $\nabla^{2\mathrm{T}}$ is the adjoint of ∇^2, and the sums are over the model time steps within the indicated intervals. Note that for the first or last 12 h of a forecast, only one sum in eq. (5) exists.

Comparisons of sensitivities with respect to ICs and LBCs must be done with the awareness that the times we have associated with the $\partial J/\partial \tilde{f}$ (e.g., t_2) refer to the discrete times at which the boundary data are provided. The boundary data at a single time actually influences the interpolated values (f_e) over the period $t_1 < t_m < t_3$, and, therefore, it may be argued that sensitivities for ICs defined at several times within that period may be appropriate for contrasting with those for LBCs;

e.g., if t_2 is the verification (end) time for a forecast, the sensitivity for the LBC at t_2 is more appropriately compared with IC sensitivities at $t_2 - 12$ h than at t_2 (the initial and end times would be identical then). In general, the appropriate times for comparison will depend on the synoptic events examined. Some examples of the flexibility required are shown in Section 4.

3. Synoptic situations

Two very different synoptic situations are considered. They were selected because the typical wind speeds will significantly affect the time it takes for boundary information to be felt in the interior, either through advection or (Rossby) wave propagation. These are the same situations selected in the examination of mesoscale dynamic balance by Errico (1990).

The initial conditions come from T42 European Center for Medium-Range Weather Forecasts (ECMWF) First GARP Global Experiment (FGGE) analysis archived at NCAR and interpolated to the MM4 grid. That grid consists of 101×76 points oriented approximately east–west × north–south, centered at 40° N and 90° W with a grid spacing of 50 km. There are 10 vertical levels, equally spaced in σ, in addition to the surface. Lateral boundary values ($\tilde{f}$) are specified as a function of time from the same spatially interpolated ECMWF analyses. Integrations

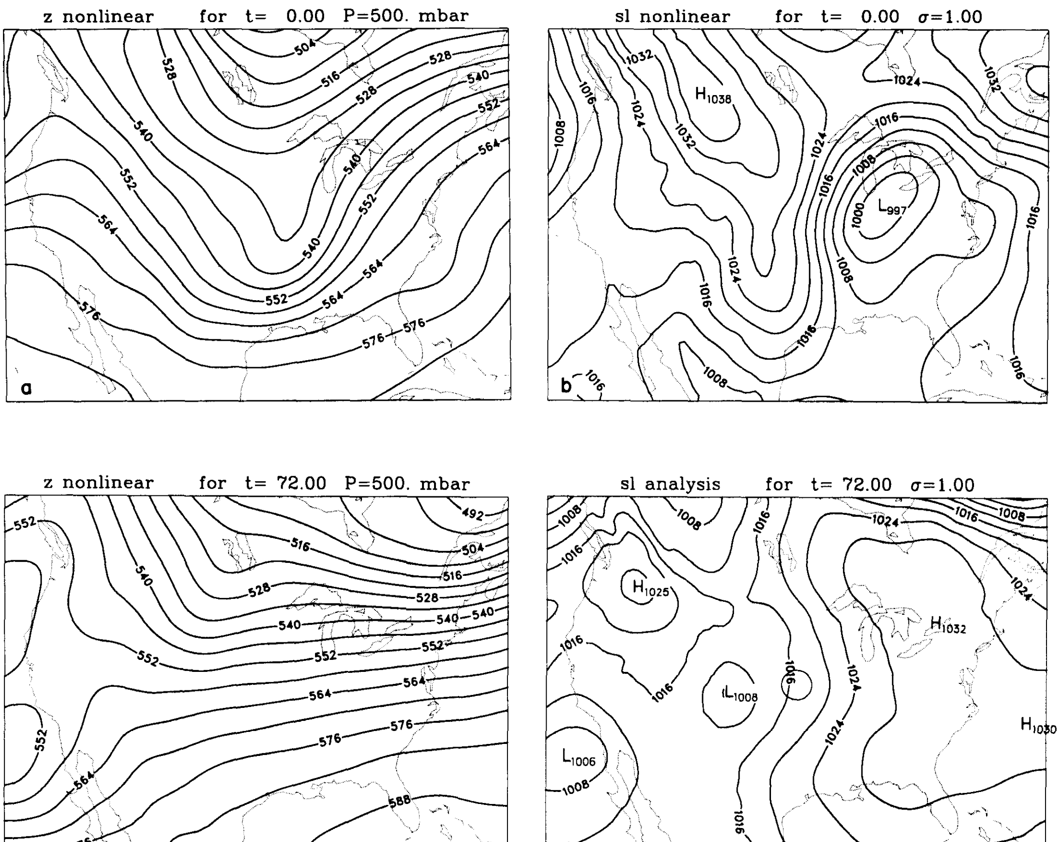

Fig. 1. The fields of 500 hPa geopotential height and sea-level pressure at the beginning (0000 UTC 14 January 1979; hour 0) and end (hour 72) of the winter case as interpolated to the MM4 grid from the ECMWF analyses. Units are dam and hPa, respectively. The circle within which the local forecast aspect is verified is indicated in (d).

of both the MM4 and adjoint model are performed with a 1-min time step.

The winter case covers the period between 0000 UTC 14 January and 0000 UTC 17 January 1979. The fields of 500 hPa geopotential height and sea-level pressure at the beginning and end of this period appear in Fig. 1. At the initial time, a surface cyclone centered over Indiana and an associated upstream upper-level trough dominate the fields. These rapidly propagate eastward until hour 48 (not shown) where the surface is dominated by anticyclones over the north-central and southeast portions of the domain with the upper level flow nearly zonal (with a slight southerly component except in the northwest quadrant of the domain). At hour 72 the surface anticyclones have propagated eastward, and a new cyclone is developing over Colorado while a 500 hPa trough appears over Montana.

The summer case covers the period between 0000 UTC 18 July and 0000 UTC 21 July 1979. The fields of 500 hPa geopotential height and sea-level pressure at the beginning and end of this period appear in Fig. 2. Throughout this period the 500 hPa flow is characterized by a quasi-stationary wave with a trough over Minnesota and a ridge over Idaho. The surface pressure field is dominated by an anticyclone which slowly propagates eastward.

Since the purpose of this paper is to show how sensitivities with regard to LBC and IC may be determined and compared and what some of their general characteristics are, attention is focused on only two forecast aspects. These are chosen for

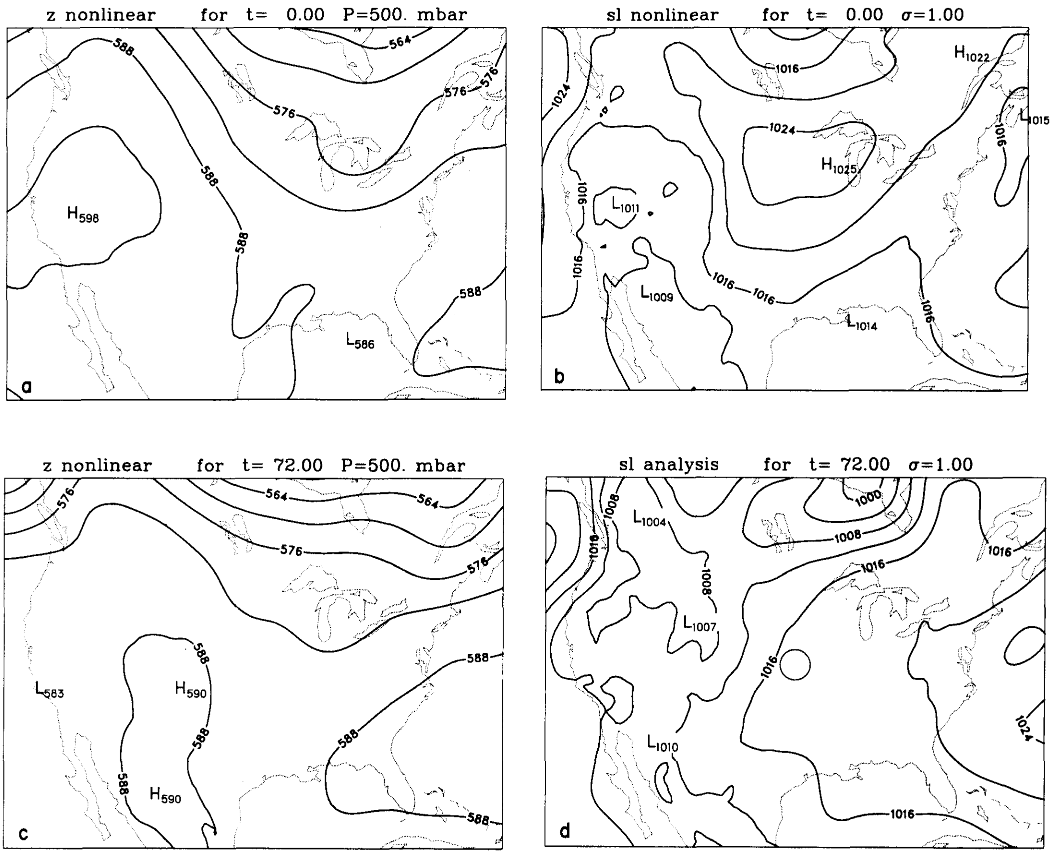

Fig. 2. Same as Fig. 1, except for the summer case beginning 0000 UTC 18 July 1979.

their location with respect to the boundaries and not for any synoptic consideration.

One forecast aspect is the domain mean square of the p^*T forecast error, computed as

$$J_1 = \frac{1}{N} \sum_{i,j,k} (p^*T - p^*T_a)^2_{i,j,k}, \tag{6}$$

where N is the number of horizontal points considered in the sum, i, j, k are northward, eastward, and downward counting grid indices, respectively, and subscript a indicates the gridded analysis value. The sum extends over the whole domain, excluding the first four points inward from any lateral boundary edge (i.e., the boundary sponge region).

The other aspect is a measure of the mean relative vorticity within a region at the center of the domain. It is computed as

$$J_2 = \frac{1}{Nf_o} \sum_{i,j,k} \Delta\sigma_k \zeta_{i,j,k}, \tag{7}$$

where f_o is the Coriolis parameter in the center of the domain, $\Delta\sigma_k$ is the vertical weighting ($\sum_k \Delta\sigma_k = 1$), and ζ is the relative vorticity determined from u and v. The sum over i, j only includes those $N = 29$ grid points within a distance $r = 150$ km from the center of the domain. This circular region is shown in Figs. 1d and 2d.

Five other forecast aspects were also examined, all measuring field characteristics near the center of the domain. These included measures of area mean p_s, summed squares of forecast error and forecast change (compared with persistence), 700 hPa height error, and change. The general statements discussed in the results and conclusion for J_2 applied to these other aspects as well.

4. Results for J_2

Selected sensitivity fields on σ-surfaces will be presented and discussed. The σ-surface value for fields referenced in the text will be indicated as a subscript. The 12-hourly defined boundary condition fields will be denoted by a tilde; absence of a tilde indicates an IC field. All sensitivities described are those for non-flux forms of the fields (e.g., v rather than p^*v) determined by decoupling the results from the flux form of the adjoint fields. The "magnitude" of a field will refer to its maximum absolute value. All times are recorded as hours prior to the verification time at which J is defined, so that the end of the 72-h forecast is hereafter denoted as hour 0 and all other times will be negative.

4.1. *Winter case*

The sensitivities of J_2 with respect to perturbations of $v_{0.35}$ (approximately on a 400 hPa surface) at selected t are presented in Fig. 3. For earlier t (more negative t indicating longer forecast durations) the sensitivity is concentrated further to the west (in accordance with the winds that tend to advect perturbations eastward), until the western boundary is reached at $t < -24$. The magnitudes of $\partial J_2/\partial v_{0.35}$ shown for hours -12 and -24 are similar. At $t = -48$, the sensitivity is concentrated along the western boundary as at $t = -24$, but the magnitude is more than a factor of 4 smaller (note that the contour interval at this time is a factor of 4 smaller than for hours -12 and -24). At $t = -72$, the sensitivity has decreased by an additional factor of 10, but the area covered by contours is increased since the contour interval has been reduced. If the contour interval at $t = -72$ were applied to all figures, similar or greater area would be covered at the other times. Similar comments apply to all sensitivities with respect to u, v, and T perturbations in the upper half of the model domain (where the wind speeds are large). The decrease in magnitude as t becomes more negative implies that perturbations of the upper tropospheric fields applied to IC at earlier times have less impact on J_2 than similar perturbations applied to IC closer to the verification time.

The sensitivity of J_2 with respect to perturbations of $\tilde{v}_{0.35}$ at $t = 0$ is presented in Fig. 4. Although this is the verification time (at the end of a forecast), boundary values specified at this time affect a forecast through their interpolation between hours 0 and -12. Note that sensitivities are concentrated near the southern and northern boundaries. In contrast, $\partial J_2/\partial \tilde{u}$ (not shown) is concentrated along the eastern and western boundaries and $\partial J_2/\partial \tilde{p}_s$ along all boundaries, but specifically at the outer edge of the sponge region. These results are in accordance with the adjoint of gravity waves as discussed in Errico and Vukićević (1992). The magnitudes of these sensitivity fields are quite small (e.g., 1% of the sensitivity with respect to v and 10% of that for p_s at $t = -12$) as expected because the barotropic circulation is only weakly affected by gravity waves (Errico and Vukićević, 1992).

The sensitivity of J_2 with respect to $\tilde{v}_{0.35}$ at other times is presented in Fig. 5. For $t = -12$, the sensitivity is concentrated in the southwest portion of the domain, similar to the location of the sensitivity with respect to $v_{0.35}$ at $t = -24$ but with half the magnitude. For $t = -24$, the magnitude of $\tilde{v}_{0.35}$ is greater than that for the corresponding IC field at that time. Also note that, within the sponge region, the structures of the sensitivity fields for IC and LBC are similar (both have a positive, negative, positive pattern). At $t = -48$, the structures are again similar, except the magnitude of the LBC field is twice that of the IC field. In other words, there are locations where a perturbation of $\tilde{v}_{0.35}$ will produce twice the impact of a same-sized perturbation of the corresponding IC field at $t = -48$. For $t = -72$, the magnitude of the sensitivity of the LBC field is reduced by a factor of 5 compared with that for $t = -48$ (but it is 5 times larger than for corresponding IC at $t = -72$), probably because the impact of LBC perturbations applied this early will be advected eastward of the region where J is measured at $t = 0$.

As is typical of most LBC fields except for $\tilde{p}_s$ or when dominated by sensitivity to gravity waves, the maximum amplitude appears within the

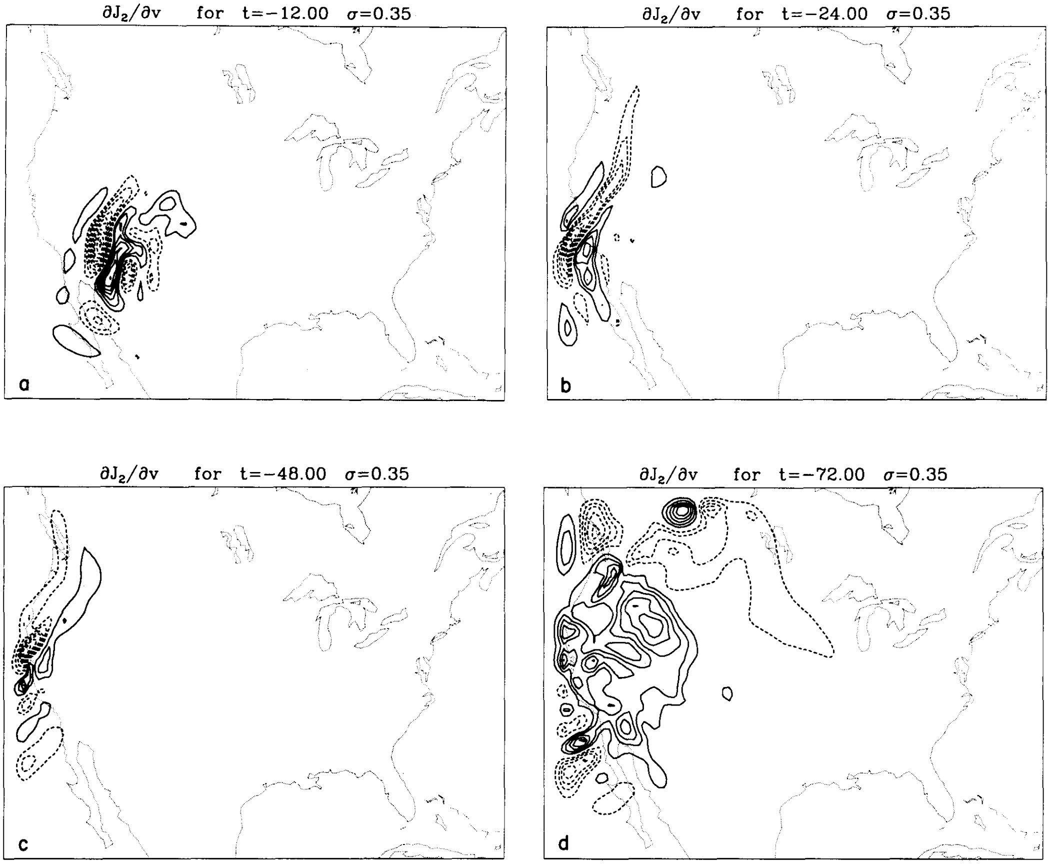

Fig. 3. The sensitivity of J_2 with respect to IC perturbations of $v_{0.35}$ at times (hours) indicated prior to the verification time for the winter case. Maximum absolute values are 93, 76, 18, and 1.4 with units 10^{-6} sm^{-1} for (a–d), respectively. Contour intervals are 10, 10, 2.5, and 0.25, respectively, in the same units. Negative-valued contours are dashed and the zero-valued contour is omitted.

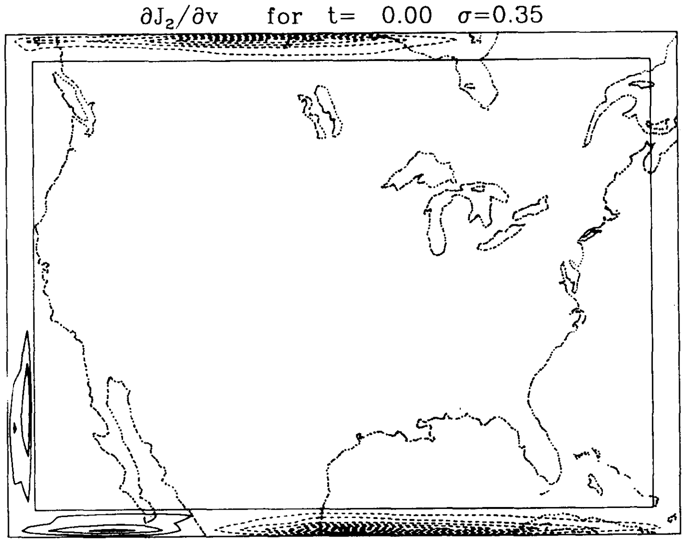

Fig. 4. As in Fig. 3, except for LBC perturbations at the verification time. The contour interval is 0.4×10^{-6} sm^{-1}.

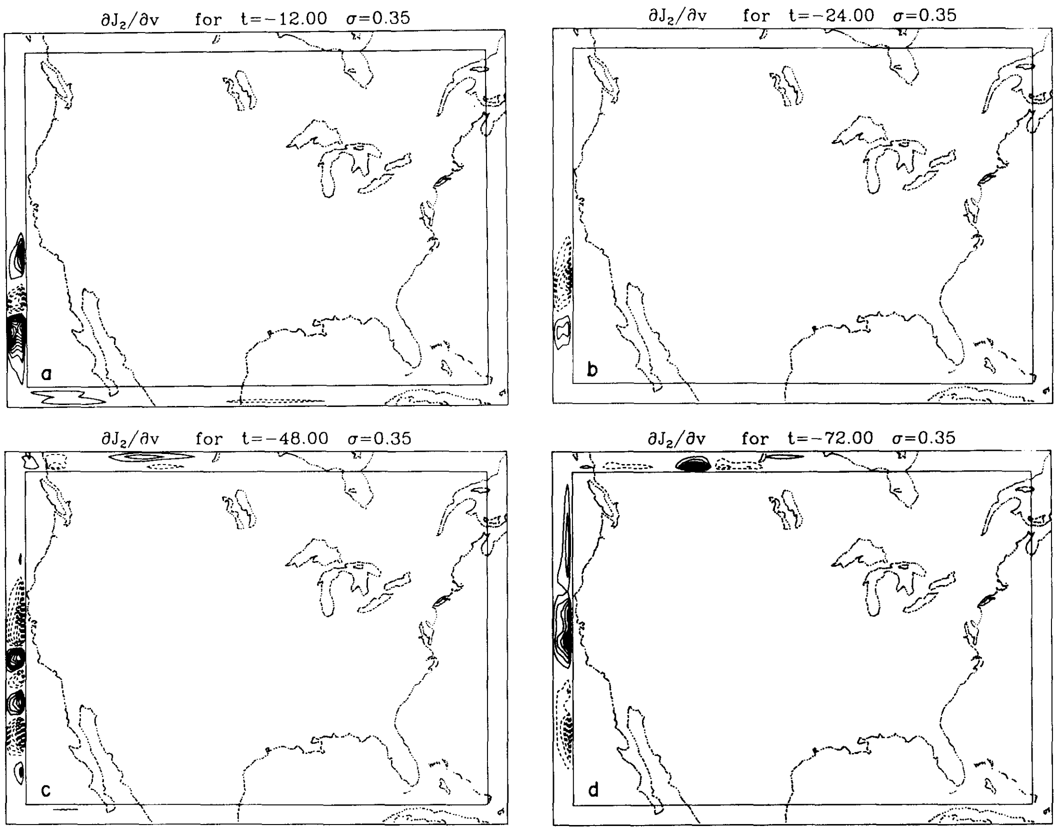

Fig. 5. As in Fig. 3, except for LBC perturbations. Maximum absolute values are 52, 150, 40, and 8 with units 10^{-6} sm^{-1} for (a–d), respectively. Contour intervals are 5, 25, 5, and 1 for (a-d), respectively, in the same units.

sponge rather than along its inner or outer edges. This is likely a result of the two contrasting processes in the sponge region that scale with the Davies and Turner (1977) weights: as the outer edge is approached, the damping time is greater (weakening the impact of LBC perturbations on perturbations of the interior flow) but the boundary forcing is greater (strengthening the direct impact by LBC perturbations).

Fields of $\partial J_2/\partial T_{0.75}$ (approximately the 775 hPa level) at selected times are presented in Fig. 6. These are intended to be representative of other low level fields with respect to the affects of horizontal advection. Since it is a lower level field, the wind advecting it is weaker, and at any time, the stronger sensitivities are found further east than for upper level fields. Magnitudes decrease by a factor of 4 between $t = -48$ and -60 during which time this sensitivity field impacts the boundary.

Magnitudes of $\partial J_2/\partial T_{0.75}$ at all examined times are greater than sensitivities with respect to u or v for any σ-level. As an example, at $t = -24$, the magnitude of $\partial J_2/\partial T_{0.75}$ is about 15 times larger than that of $\partial J_2/\partial v_{0.35}$, indicating that a perturbation of 1 K at the point of maximum sensitivity for $T_{0.75}$ will create a change of J_2 after a 24-h forecast that is 15 times larger than the change produced by a 1 ms^{-1} perturbation of $v_{0.35}$ at its point of maximum sensitivity. Equivalently, to obtain the same

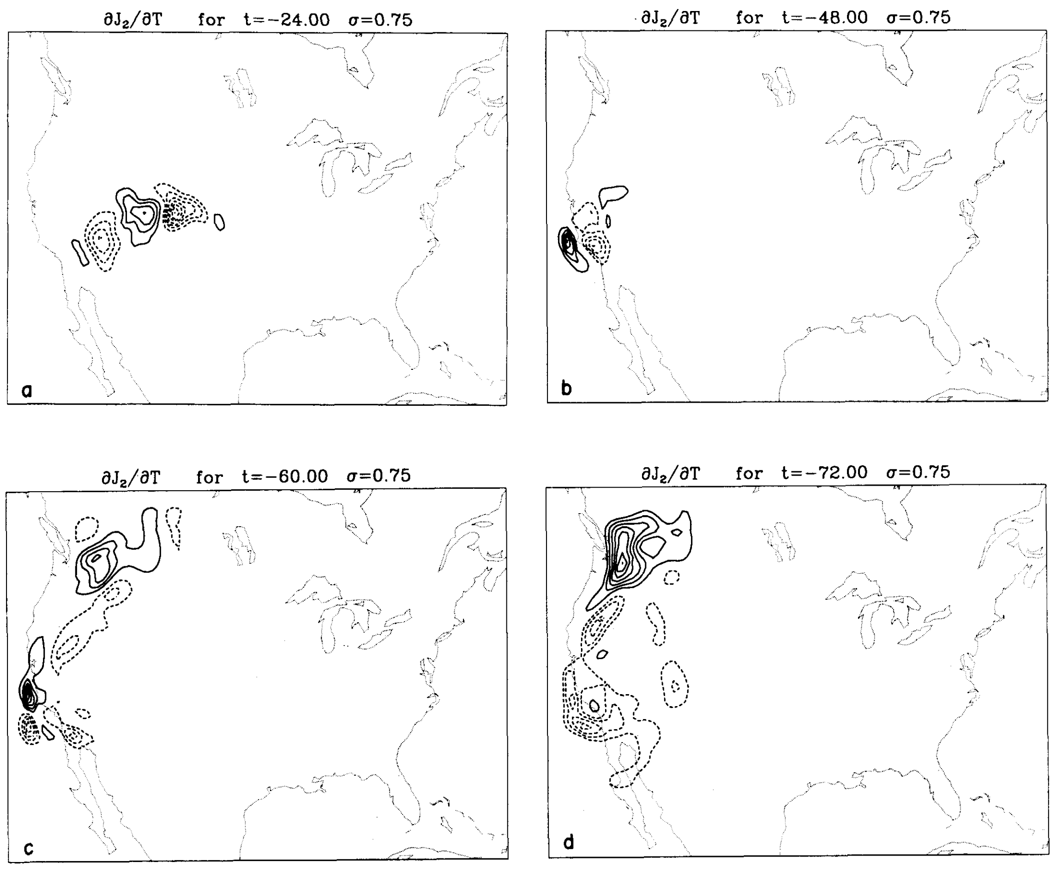

Fig. 6. The sensitivity of J_2 with respect to IC perturbations of $T_{0.75}$ at times (hours) indicated prior to the verification time for the winter case. Maximum absolute values are 14, 5.1, 1.2, and 0.7 with units 10^{-4} K^{-1} for (a–d), respectively. Contour intervals are 2, 1, 0.2, and 0.1, respectively, in the same units. Negative-valued contours are dashed and the zero-valued contour is omitted.

impacts on J_2 from perturbations at the points in question, the $v_{0.35}$ perturbation would have to be 15 ms^{-1} for each 1 K perturbation of $T_{0.75}$.

The sensitivities of J_2 with respect to $\tilde{T}_{0.75}$ at selected times appear in Fig. 7. At $t = -24$, the sensitivity is concentrated in the southwest portion of the domain although the corresponding IC field at this time has greatest amplitude still far from the boundary, with more than 5 times the magnitude. For $t = -48$, the magnitude of the sensitivity with respect to the LBC field is twice that for the IC field at the same time, and the regions of maximum amplitudes are in close proximity. For $t = -72$, the LBC pattern looks more like that for the IC at $t = -60$ than for the IC at $t = -72$. The magnitudes for these three fields are all similar; there are not large contrasts as for the $v_{0.35}$ field. For $t = -72$, the magnitude of $\partial J_2/\partial \tilde{T}_{0.75}$ is approximately 8 times larger than for $\partial J_2/\partial \tilde{v}_{0.35}$ (in standard units), similar to the comparison for the IC conditions. The temporal behaviors of lower tropospheric sensitivity fields are similar to those for the upper-level fields except that the time it takes to impact the boundary is greater. Therefore, there exists a range of times for which either IC or LBC may be more important at either higher or lower levels.

Fields of $\partial J_2/\partial p_s$ appear in Fig. 8. The temporal propagation of the pattern is similar to that for other low level fields. Magnitudes of the fields are

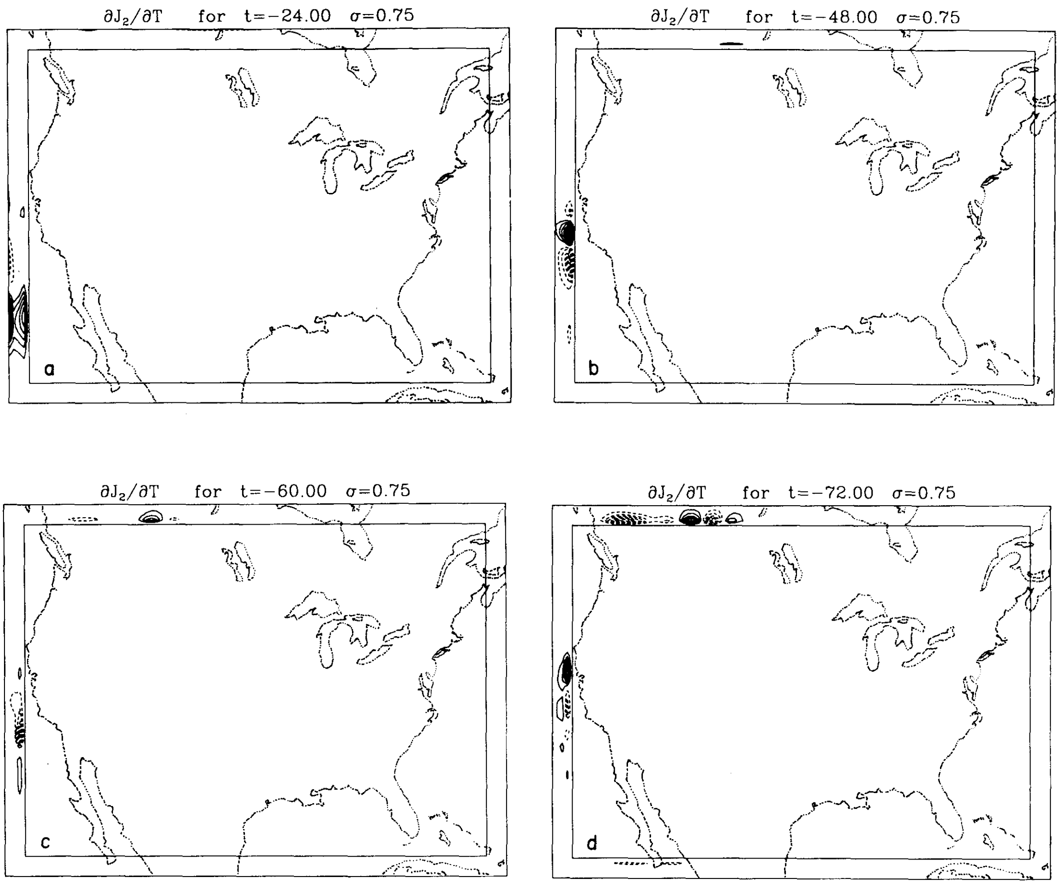

Fig. 7. As in Fig. 6, except for LBC. Maximum absolute values are 2.8, 10, 2.5, and 0.6 with units $10^{-4}\,\mathrm{K}^{-1}$ for (a–d), respectively. Contour intervals are 0.4, 1.0, 0.5, and 0.1, respectively, in the same units.

approximately one-tenth those for $T_{0.75}$ at the same times (if 1 hPa is considered equivalent to 1 K).

The sensitivities of J_2 with respect to $\tilde{p}_s$ appear in Fig. 9. At all times presented, magnitudes are at least three times those for $\partial J_2/\partial p_s$ at the same times. Unlike the other boundary fields, this one is always greatest at the outer edge of the boundary. We offer no explanation of this fact, but emphasize that this is common with all the sensitivities we have investigated, even for other synoptic conditions.

4.2. *Summer case*

The sensitivity of J_2 with respect to selected IC fields at selected times for the summer case appears in Fig. 10.

The field of $\partial J_2/\partial v_{0.35}$ appears to be just nearing the boundary at $t = -48$. For this case it is the northern boundary in contrast to the winter case (Fig. 3). Although this boundary is closer to the region where J_2 is evaluated, the weaker wind speed results in more than a factor of two slower propagation of the sensitivity. The magnitude at $t = -24$ is twice that for the winter case and at $t = -48$ a factor of 6 larger, although this latter factor is best attributable to the fact that, in the winter case, the impact with the boundary has already occurred.

The field of $\partial J_2/\partial T_{0.75}$ at $t = -48$ appears in Fig. 10c. The magnitude is similar to that for the winter case, but the region of significant perturbation is almost colocated with the circle where J_2 is evaluated.

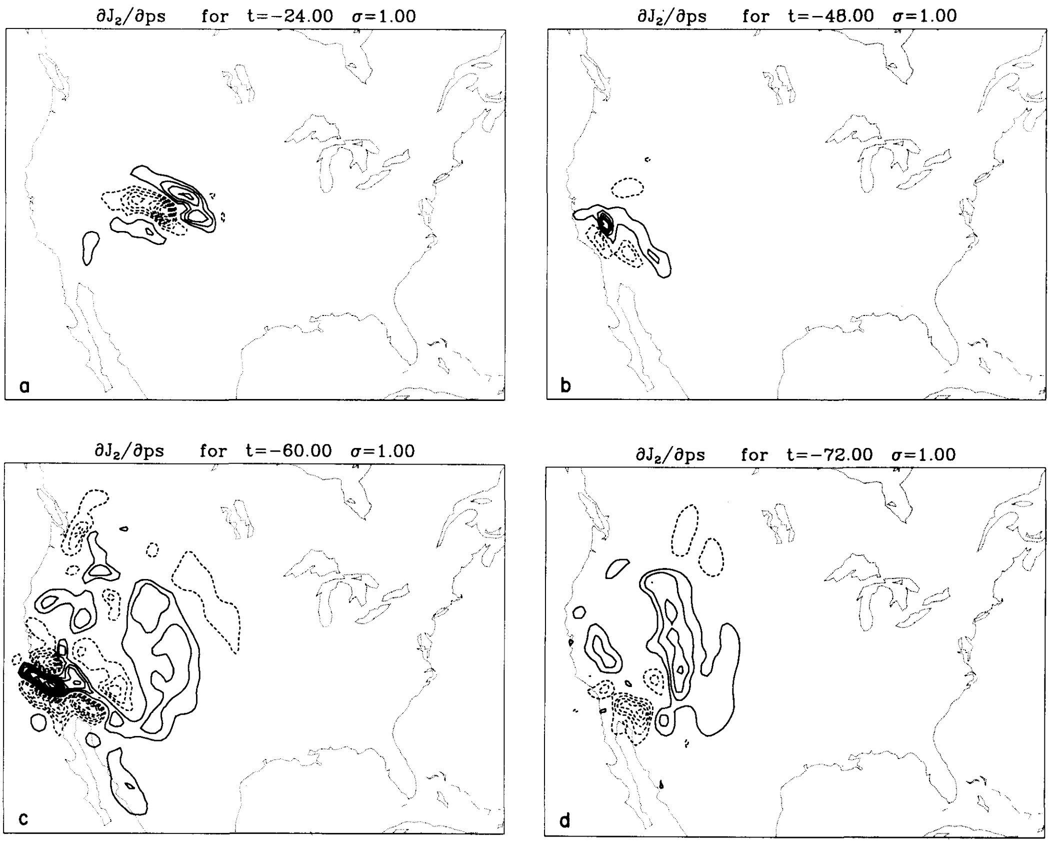

Fig. 8. The sensitivity of J_2 with respect to IC perturbations of p_s at times (hours) indicated prior to the verification time for the winter case. Maximum absolute values are 20, 6.3, 1.1, and 0.6 with units $10^{-5}\,\mathrm{hPa}^{-1}$ for (a–d), respectively. Contour intervals are 2.5, 1, 0.1, and 0.1, respectively, in the same units. Negative-valued contours are dashed and the zero-valued contour is omitted.

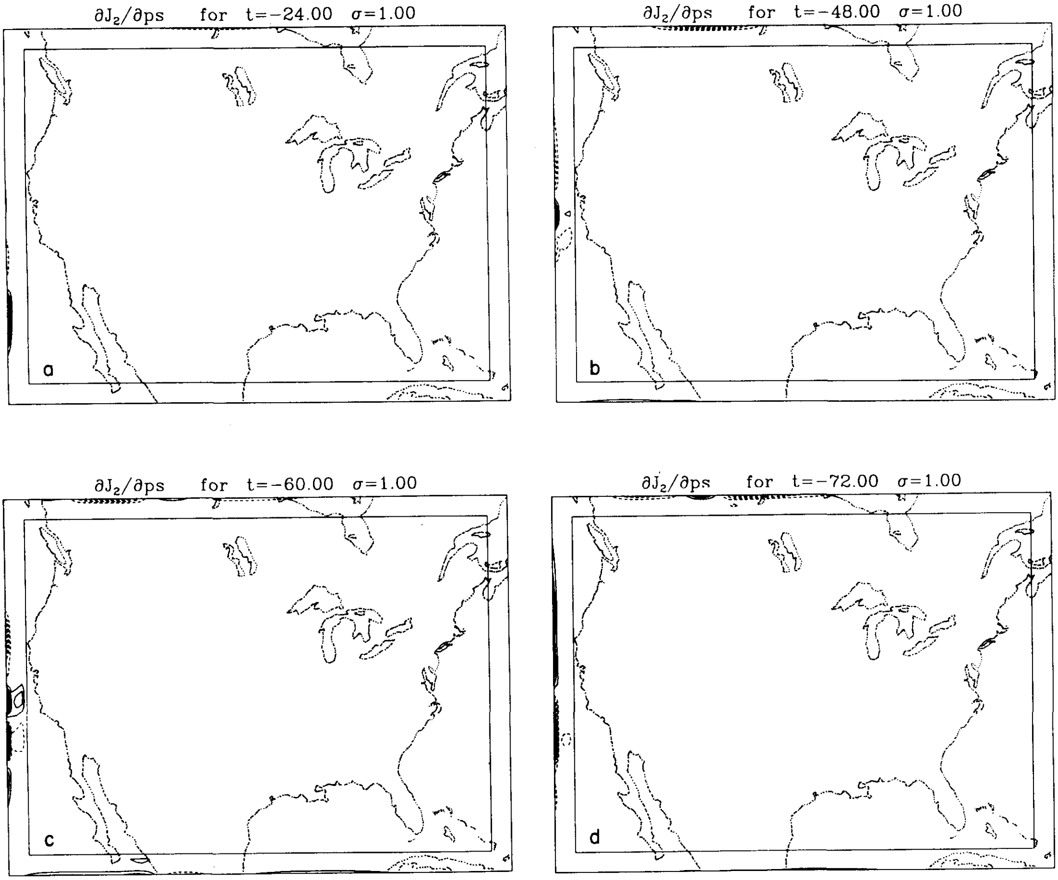

Fig. 9. As in Fig. 8, except for LBC. Maximum absolute values are 75, 22, 10, and 4 with units 10^{-5} hPa^{-1} for (a–d), respectively. Contour intervals are 10, 4, 1, and 0.5, respectively, in the same units.

The field of $\partial J_2/\partial p_s$ at $t = -48$ is presented in Fig. 10d. Its magnitude is one-half that for the winter case at the same hour and it is much less localized.

Sensitivities with respect to the LBC fields corresponding to those in Fig. 10 appear in Fig. 11. At $t = -24$, $\partial J_2/\partial \tilde{v}_{0.35}$ appears to still have the signature of gravity waves analogous to those attributed to Fig. 4. By $t = -48$, the magnitude of $\partial J_2/\partial \tilde{v}_{0.35}$ has increased and the large amplitudes are localized in agreement with Fig. 10b. At $t = -48$, $\partial J_2/\partial \tilde{T}_{0.75}$ still has weak amplitude, in agreement with the slow propagation attributed to Fig. 10c. An equivalent result holds for $\partial J_2/\partial \tilde{p}_s$ compared with Fig. 10d.

5. Results for J_1

At $t = 0$, J_1 is only dependent on p^*T. Specifically,

$$\frac{\partial J_1}{\partial p^*T} = \frac{2}{N}(\overline{p^*T} - p^*T_a) \tag{8}$$

for each point, where the overline signifies the control forecast values. For this J, the sensitivity field at the verification time is equivalent to a scaled (factor of $2/N$) field of forecast error. These errors are non-zero if either the T or p_s forecast is in error. In fact, the sensitivity with respect to p_s is greater

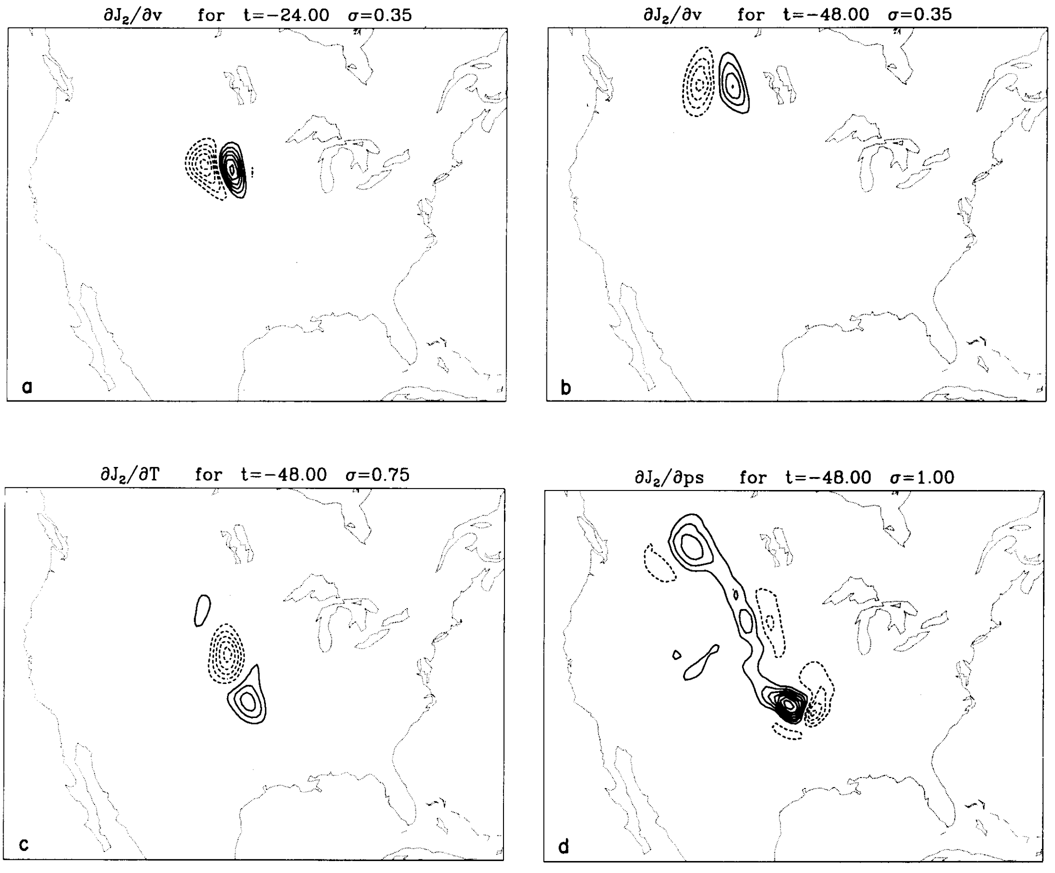

Fig. 10. The sensitivity of J_2 with respect to IC perturbations of the indicated fields at times (hours) indicated prior to the verification time for the summer case. Maximum absolute values are 160×10^{-6} sm^{-1}, 108×10^{-6} sm^{-1}, 5.3×10^{-4} K^{-1}, and 3.7×10^{-5} hPa^{-1} for (a–d), respectively. Contour intervals are (a–b) 25, (c) 1, and (d) 0.5, with the same respective scaling by tens and units. Negative-valued contours are dashed and the zero-valued contour is omitted.

because a single p_s perturbation affects all σ-levels, unlike a single T perturbation.

5.1. Winter case

The field of $\partial J_1/\partial p^* T_{0.75}$ at the verification time appears in Fig. 12. This is computed from forecast T errors as large as 2.8 K and p_s errors as large as 0.9 hPa. Errors are greater in the east, in agreement with the sweeping effect discussed in Section 4.

The sensitivity of J_1 with respect to $v_{0.35}$, $\tilde{v}_{0.35}$, $T_{0.75}$, and $\tilde{T}_{0.75}$ at $t = -24$ appears in Fig. 13. There is some matching of regions of large amplitude for sensitivities of $v_{0.35}$ and $\tilde{v}_{0.35}$ fields (both have large positive values over Saskatchewan and large negative values west of Baja California). Matching of regions is less apparent for the $T_{0.75}$ and $\tilde{T}_{0.75}$ fields. Magnitudes of the LBC fields are about 4 times those of corresponding IC fields at the same time, although for $\tilde{p}_s$ (not shown) it is 40 times greater. Note that the magnitudes of the $\partial J_2/\partial T_{0.75}$ and $\partial J_2/\partial \tilde{T}_{0.75}$ fields are 4 times those of the corresponding fields for $v_{0.35}$ (if 1 K is considered equivalent to 1 ms^{-1}. Similar comments apply at $t = -48$ (not shown).

In Fig. 14, the same fields are presented as in

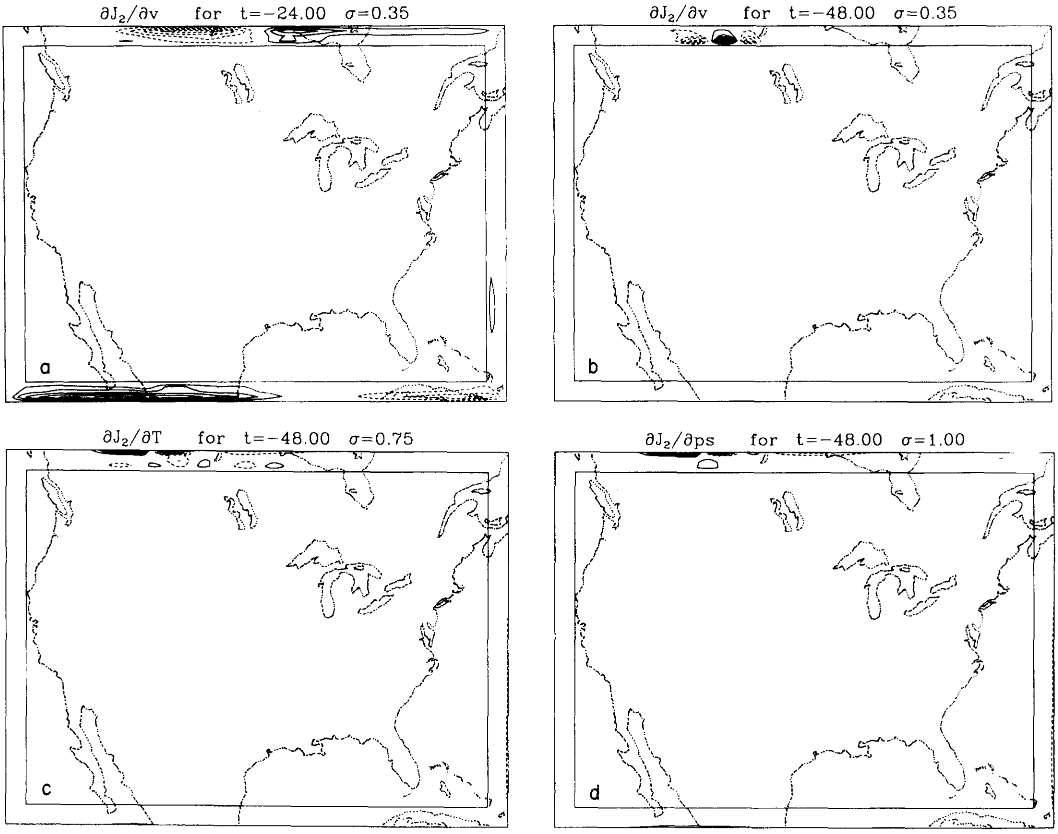

Fig. 11. As in Fig. 10, except for LBC. Maximum absolute values are 3×10^{-6} sm^{-1}, 80×10^{-6} sm^{-1}, 0.6×10^{-4} K^{-1}, and 21×10^{-5} hPa^{-1} for (a–d), respectively. Contour intervals are 0.5, 20, 0.1, and 2.5 with the same respective scaling by tens and units.

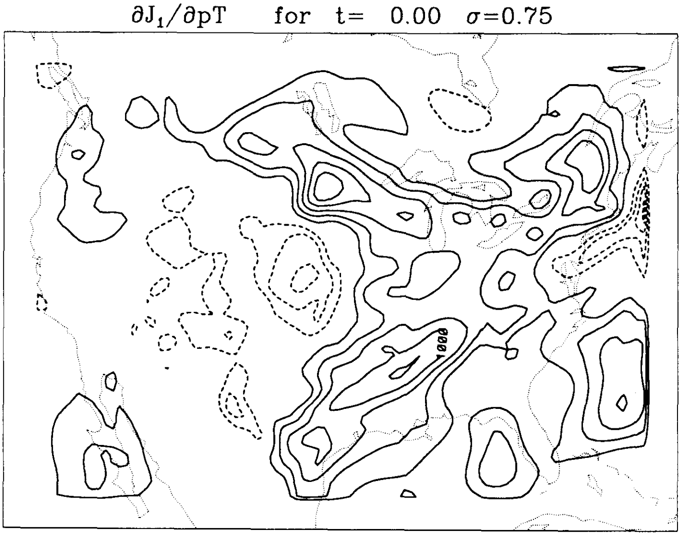

Fig. 12. The sensitivity of J_1 with respect to IC perturbations of the $p^*T_{0.75}$ field at the verification time for the winter case. The contour interval is 2.5×10^{-3} (dimensionless). Negative-valued contours are dashed and the zero-valued contour is omitted.

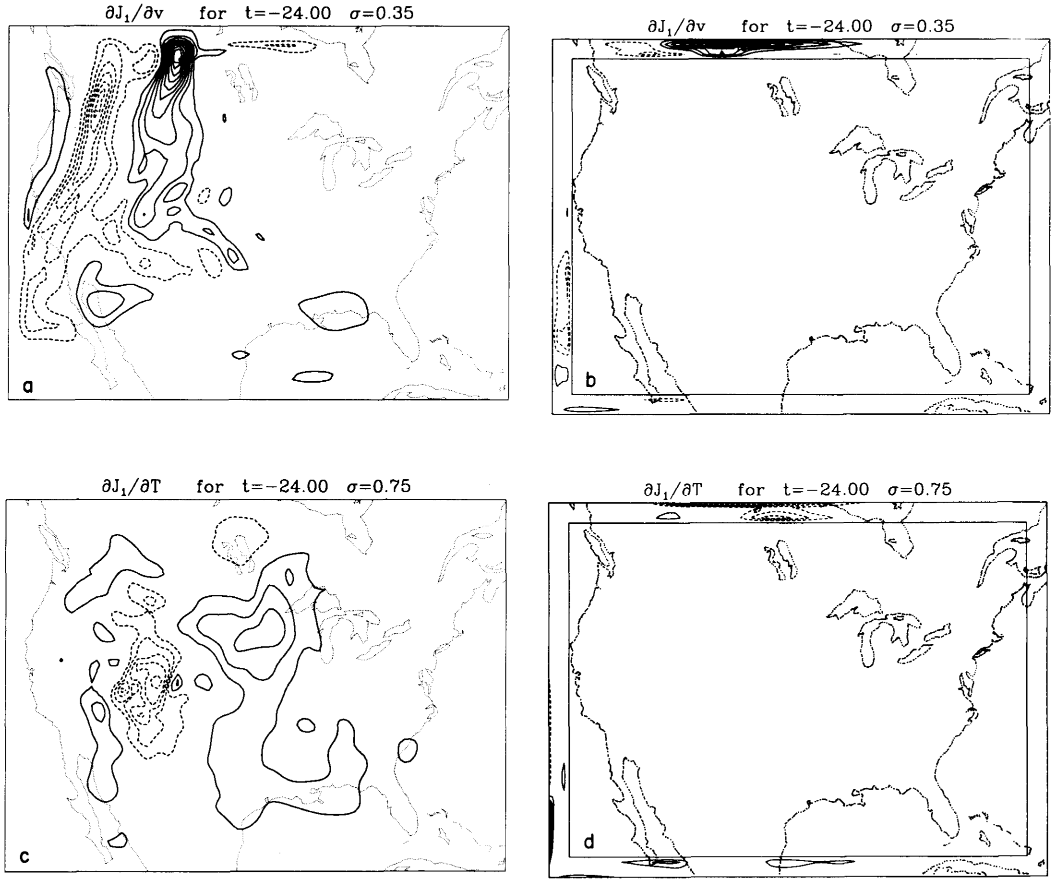

Fig. 13. The sensitivity of J_1 with respect to IC and LBC perturbations of the indicated fields at 24 h prior to the verification time for the winter case. Maximum absolute values are 0.55 $(\mathrm{K\,hPa})^2\,\mathrm{sm}^{-1}$, 2.0 $(\mathrm{K\,hPa})^2\,\mathrm{sm}^{-1}$, 2.3 K hPa^2, and 8 K hPa^2 for (a–d), respectively. Contour intervals are 0.05, 0.25, 0.4, and 1.0 in the same respective units. Negative-valued contours are dashed and the zero-valued contour is omitted.

Fig. 13 but at $t = -72$. Sensitivities with respect to the IC fields are located in the far west, consistent with the effects of advection. The magnitude of $\partial J_2/\partial T_{0.75}$ has increased slightly compared with $t = -24$, but those for the other fields shown have decreased. This means that it takes a perturbation of greater magnitude (or a structure whose sign and magnitude are more in tune with those of the sensitivity field) to obtain the same magnitude effect from an insertion at $t = -72$ than at $t = -24$. This agrees with the behavior of perturbations usually reported for the MM4 (Errico and Baumhefner, 1987; Vukićević and Errico, 1990): their magnitudes generally decrease in time and area covered, so it takes a large perturbation to obtain a significant domain averaged effect after 72 h. Unlike the example offered in Vukićević and Errico (1990), if the LBC perturbation is removed after only 12 h, the perturbation dies during the next 60 h, just as it would for an IC perturbation.

5.2. *Summer case*

In Fig. 15, the same fields as in Fig. 14 are presented but for the summer case. Sensitivities with respect to ICs are more spread out than for the winter case. For the wind field (LBC and IC) they are several times stronger, but for the T field, magnitudes for both cases are similar. Magnitudes

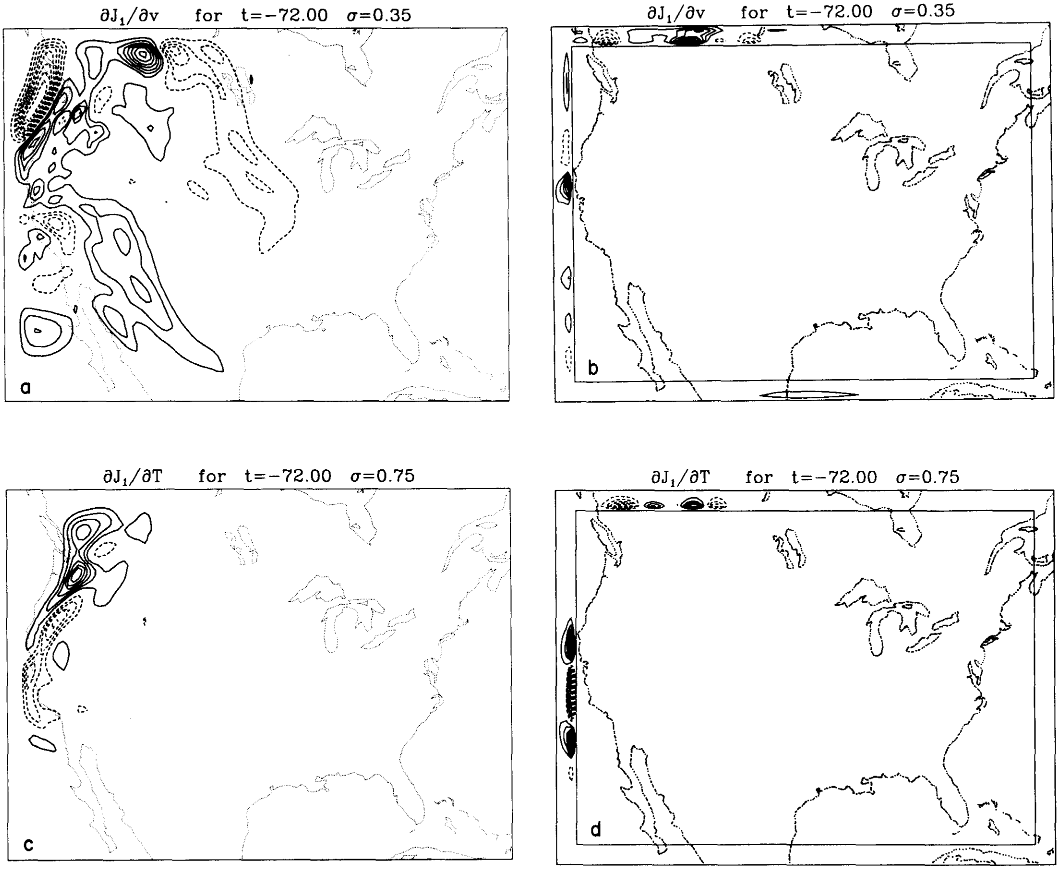

Fig. 14. As for Fig. 13, except for hour −72. Maximum absolute values are 0.08 (K hPa)^2 sm^{-1}, 0.35 (K hPa)^2 sm^{-1}, 3.5 K hPa^2, and 3.0 K hPa^2 for (a–d), respectively. Contour intervals are 0.01, 0.05, 0.5, and 0.5 in the same respective units.

of all IC fields for the summer case are two to three times corresponding fields at $t = -12$; i.e., the sensitivity with respect to IC perturbations is greater for longer duration forecasts, which is the opposite relation observed for the winter case. Apparently for the summer case there is more time for perturbations to grow since they are swept out by the boundaries more slowly. The sensitivity with respect to LBC fields is highly concentrated, with magnitudes comparable to those for the IC (greater for some fields, less for others).

6. Summary

If a forecast aspect is measured at a verification time $t = 0$ in a small portion of a forecast domain and far from the lateral boundaries, the only sensitivity of the aspect with respect to LBC defined at times not long before $t = 0$ must be due to gravity wave propagation (or some computational mode). For a Davies and Turner (1977) LBC formulation, this sensitivity appears to be concentrated along the outer edge of the sponge region.

Sensitivity with respect to LBC increases sharply at the time a feature of significant IC sensitivity impacts with the LBC region. This time is dependent on wind speeds and vertical levels (as the winds are). Also at this time, the IC sensitivity may decrease sharply although not disappear entirely. It is as though the primary feature has passed through the boundary (along a backward trajectory in time, since we are speaking of sensitivity), and all that remain are secondary

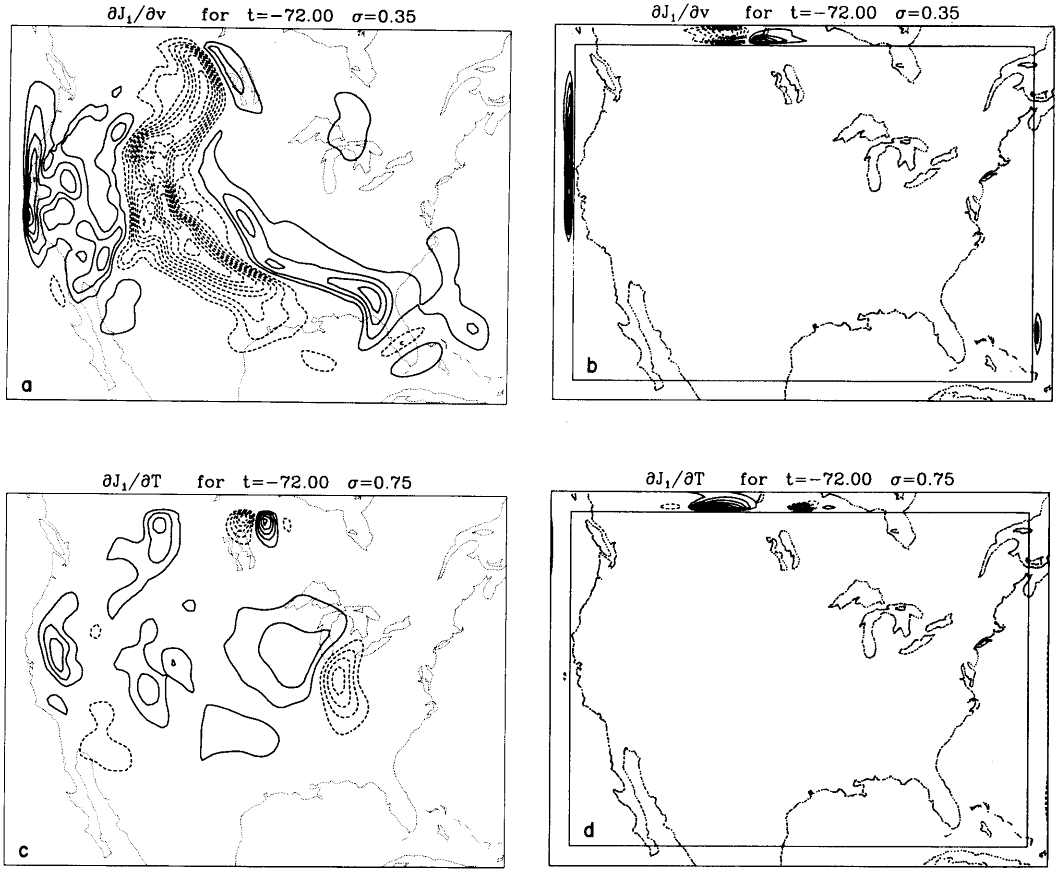

Fig. 15. As for Fig. 14, except hour −72 for the summer case. Maximum absolute values are 0.18 (K hPa)^2 sm^{-1}, 0.9 (K hPa)^2 sm^{-1}, 2.5 K hPa^2, and 4.5 K hPa^2 for (a–d), respectively. Contour intervals are 0.025, 0.1, 0.5, and 0.5 in the same respective units.

features; i.e., regions where IC perturbations would impact the forecast aspect, but with less magnitude than comparable perturbations in a shorter duration forecast (beginning at a time closer to $t = 0$). Sensitivity is naturally concentrated at inflow boundaries, although outflow sensitivities can be seen for waves that propagate against the flow (e.g., gravity waves near hour 0).

The time at which sensitivity with respect to a LBC field has greater magnitude than for a corresponding IC field will typically be later for a winter case than for a summer one, since the relevant time scales should scale somewhat with wind speeds. In the winter at upper levels, perturbations can propagate from the Pacific coast to the center of the US in less than 24 h, so a forecast aspect that is measured in the center of the country and is especially sensitive to upper-level conditions may be more sensitive to LBC than IC for forecasts longer than 24 h. For summer cases, sensitivities with respect to IC should remain more important out to several days.

Although we have related the propagation of sensitivity fields to the winds, we do not wish to imply that the process is simply advection. One counter example that has been presented here is the sensitivity with respect to gravity waves, which propagates at the speed of those waves. Other examples are shown in Errico and Vukićević, 1992 (Figs. 6 and 20) that clearly relate sensitivity fields to quasi-geostrophic waves, and therefore to their propagation characteristics. On the synoptic scales investigated, the propagation speeds of these Rossby-type waves are strongly dependent on wind speeds, so we have not attempted to distinguish between wave propagation or advection in our investigation here.

In our experience with the Davies and Turner (1977) scheme, sensitivities of aspect measures with respect to perturbations of the LBC fields of the surface pressure are usually much greater along the outer edge of the sponge region than at other points in the sponge. With respect to the LBC wind fields, the greatest sensitivity is usually found somewhere between the inner and outer edge. For either type of LBC field, the gradients of the sensitivity field normal to the edges are often very large.

Although the magnitudes of sensitivities with respect to LBC fields may be larger than for corresponding IC fields, the net effect of perturbations to the LBC fields may be less. Since the net effect on an aspect measure is determined by the sum of contributions from all points, the fact that the IC are defined at more points than the LBC may tend to make the magnitudes of the two net sensitivities more similar. The structures of perturbations, as well as the sensitivity fields, must be considered when determining net effects.

We have considered that regions of significant sensitivity are those enclosed by non-zero contours in the figures; i.e., grid points where the absolute values of a field are not less than approximately 20% of the maximum absolute value for the field. In the experiments where the forecast aspect was the mean barotropic vorticity over a small area, regions of significant sensitivity remained small at all times until the region was at the lateral boundary. For longer times the secondary sensitivities are observed, and their scales are less constrained. The regions of significant sensitivity for the LBC were also small. Even for the forecast aspect which was the forecast error evaluated over the whole domain, the scales of these regions were small if measured in terms of gradients or typical distances between high and low values. For both aspects, a typical scale for the sensitivity fields may be on the order of 500 km.

For many forecast sensitivity, predictability, and observing system simulation experiments, IC or LBC perturbations are introduced using random numbers (e.g., Anthes et al., 1985). If the number of forecast aspects measured is very limited, as is usually necessary, then sensitivity will likely be underestimated because the regions of primary sensitivity are small and the random perturbations from point to point will result in much cancellation to the net sensitivity. If smoothing of the random fields is performed prior to their application (e.g., Errico and Baumhefner, 1987; Vukićević and Errico, 1990), then the sensitivities will also likely be underestimated because the perturbations of a single sign will likely overlap regions of sensitivity of both signs, again resulting in significant cancellation.

In order to estimate the maximum sensitivity, it is necessary to first determine the fields of sensitivity using the model's adjoint. Perhaps in some idealized flows, the sensitivity patterns may be ascertained without such calculation; however, for real synoptic situations, it is hard to imagine constructing the figures shown in this report without actually performing the numerical adjoint calculations.

7. Acknowledgments

T. Vukićević and K. Raeder are funded through the National Aeronautics and Space Administration's (NASA) Earth Observing System (EOS) Interdisciplinary Science Investigation entitled "NCAR project to interface climate modeling on global and regional scales with EOS observations" working on problems and development of data assimilation. Participation at the Workshop on Adjoint Applications in Dynamic Meteorology was partially funded by NASA and the National Science Foundation (NSF). The manuscript was prepared by Lydia Harper.

REFERENCES

Anthes, R. A., Hsie, E.-Y. and Kuo, Y.-H. 1987. Description of the Penn State/NCAR Mesoscale Model Version 4 (MM4). NCAR Technical Note, NCAR/TN – 282 + STR, 66 pp. [Available from the National Center for Atmospheric Research, P.O. Box 3000, Boulder, CO 80307, USA.]

Anthes, R. A., Kuo, Y.-H., Baumhefner, D. P., Errico, R. M. and Bettge, T. W. 1985. Predictability of mesoscale motions. *Issues in Atmospheric and Oceanic Modelling, Part B, Advances in Geophysics 28*, 159–202.

Davies, H. C. and Turner, R. E. 1977. Updating prediction models by dynamical relaxation: An examination of the technique. *Quart. J. Roy. Meteor. Soc. 103*, 225–245.

Errico, R. M. and Baumhefner, D. P. 1987. Predictability experiments using a high-resolution limited-area model. *Mon. Wea. Rev. 115*, 488–504.

Errico, R. M. 1990. An analysis of dynamic balance in a mesoscale model. *Mon. Wea. Rev. 118*, 558–572.

Errico, R. M. and Vukićević, T. 1992. Sensitivity analysis using an adjoint of the PSU-NCAR mesoscale model. *Mon. Wea. Rev. 120*, 1644–1660.

Errico, R. M., Vukićević, T. and Raeder, K. 1993. Examination of the accuracy of a tangent linear model. *Tellus 45A*, 462–477.

Hall, M. C. G. and Cacuci, D. G. 1983. Physical interpretation of adjoint functions for sensitivity analysis of atmospheric models. *J. Atmos. Sci. 40*, 2537–2546.

Hall, M. C. G., Cacuci, D. G. and Schlesinger, M. E. 1982. Sensitivity analysis of a radiative convective model by the adjoint method. *J. Atmos. Sci. 39*, 2038–2050.

Vukićević, T. and Errico, R. M. 1990. The influence of artificial and physical factors upon predictability estimates using a complex limited-area model. *Mon. Weather Rev. 118*, 1460–1482.

Vukićević, T. and Errico, R. M. 1993. Linearization and adjoint of parameterized moist diabatic processes. *Tellus 45A*, 493–510.